Scripta Materialia 186 (2020) 202–207

Contents lists available at ScienceDirect

Scripta Materialia

journal homepage: www.elsevier.com/locate/scriptamat

# Thermal stabilization of metal matrix nanocomposites by nanocarbon reinforcements

A. Bachmaier[a,*], A. Katzensteiner[a], S. Wurster[a], K. Aristizabal[b], S. Suarez[b], R. Pippan[a]

[a] Austrian Academy of Sciences, Erich Schmid Institute, Jahnstrasse 12, 8700 Leoben, Austria
[b] Department of Materials Science, Saarland University, D-66123 Saarbrücken, Germany

ARTICLE INFO

*Article history:*
Received 23 March 2020
Revised 30 April 2020
Accepted 5 May 2020
Available online 2 June 2020

*Keywords:*
Severe plastic deformation
Thermal stability
Nanocomposite
Nickel
Silver

ABSTRACT

Metal matrix composites reinforced by nanocarbon materials, such as carbon nanotubes or nanodiamonds, are very promising materials for a large number of functional and structural applications. Carbon nanotubes and nanodiamonds-reinforced metal matrix nanocomposites with different concentrations of the carbon phase were processed by high-pressure torsion deformation and the evolving nanostructures were thoroughly analyzed by electron microscopy. Particular emphasis is placed on the thermal stability of the nanocarbon reinforced metal matrix composites, which is less influenced by the amount of added nanocarbon reinforcements than by the nanocarbon reinforcement type and its distribution in the metal matrix.



Metal matrix composites (MMCs) are a class of materials, which have been in the focus of interest in the material science community for quite some time [1]. Very important for their structural and mechanical supremacy over pure metals is a homogenous distribution of the second phase particles. Several methods are used to achieve such a distribution, such as stir casting, infiltration or powder processing, which impose strong forces and high temperatures on the composites [2]. High-pressure torsion (HPT) as a severe plastic deformation (SPD) technique is known for imposing large strains on the material, which cause a reduction of the grain size and an increase of strength of the deformed materials [3]. HPT can also be used for optimizing the distribution of second phase particles in MMCs [4].

Carbon nanotubes (CNTs) or nanodiamonds (ND) from the class of nanocarbon materials are of great interest as second phase materials, since they offer superior mechanical and thermal properties increasing the tensile strength, microhardness and thermal stability of the matrix material. On the other side, they tend to form large agglomerates which can cause a deterioration of the mechanical properties, thus, a homogeneous distribution and a dissolution into smaller agglomerates or single nanocarbon particles is essential [5].

Efforts to improve the thermal stability by adding nanocarbon reinforcements to metallic matrices have already been made [6–11]. In [10] it was shown that CNT reinforced Ni composites exhibited an improved thermal stability in comparison to pure Ni samples processed in the same way. The goal of this study is to get a better understanding on the influence of the amount, type and distribution of nanocarbon reinforcements in the metal matrix on the thermal stability. Regarding the high cost of nanocarbon reinforcements, another main question that has to be answered is what minimum amount is necessary to stabilize the structure.

Fully dense bulk ultrafine grained or nanocrystalline MMCs can be processed by HPT-deformation and the distribution of CNT or ND agglomerates can be altered with processing conditions [12–14]. To obtain nanocrystalline MMCs with different amount and also two different distributions of nanocarbon reinforcements in the metallic matrix, powder blends of Ni (Alfa Aesar, mesh −325, dendritic) and CNTs (CCVD grown, Graphene Supermarket, USA) with 0.1, 0.25, 0.5, 1, 2 and 3wt% CNTs were HPT processed at a deformation temperature of 200°C and with a two-temperature deformation process (deformation temperature of 400°C followed by 200°C) as described in [12].

In general, the CNT distribution homogeneity is improved on a µm length scale after the two-temperature deformation process. As an example, Fig. 1 shows the final distribution of the CNTs in Ni-MMCs with 0.1, 1, 2 and 3wt% CNTs. The images, which are obtained by binarisation of scanning electron microscope (SEM) micrographs, display only CNT agglomerates (in black) for better visualization. After HPT-deformation at 200°C (upper row), the size of the CNT agglomerates in the Ni matrix shows a large variation

* Corresponding author:
*E-mail address:* andrea.bachmaier@oeaw.ac.at (A. Bachmaier).

https://doi.org/10.1016/j.scriptamat.2020.05.014

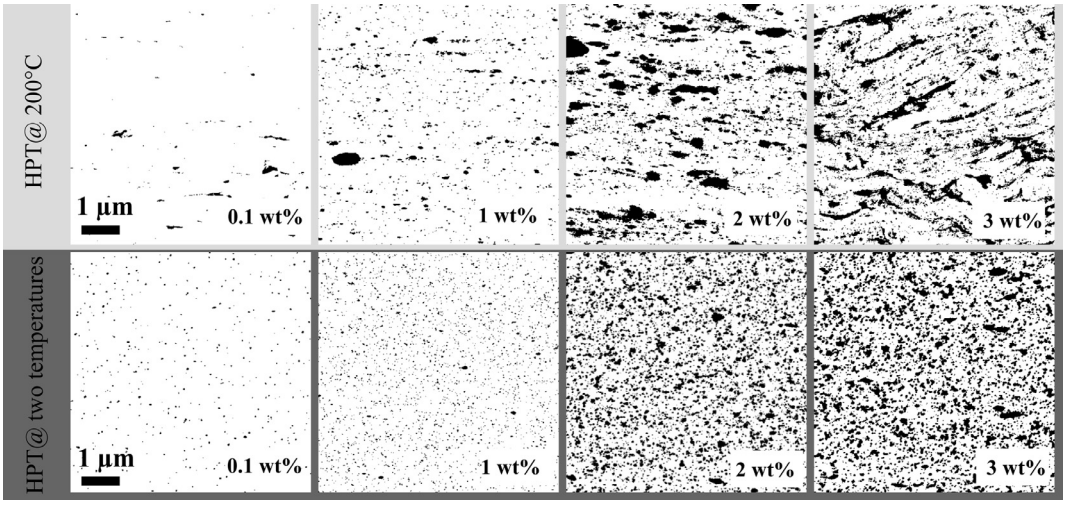


**Fig. 1.** Binarised images from SEM micrographs of Ni-MMCs with 0.1, 1, 2 and 3 wt% CNTs. The dark regions correspond to CNT agglomerates. The scale bar is the same in each image. The HPT samples were deformed at 200°C for 30 rotations (upper row) and with a two-temperature process (lower row, 30 rotations at 400°C, followed by 10 rotations at 200°C).

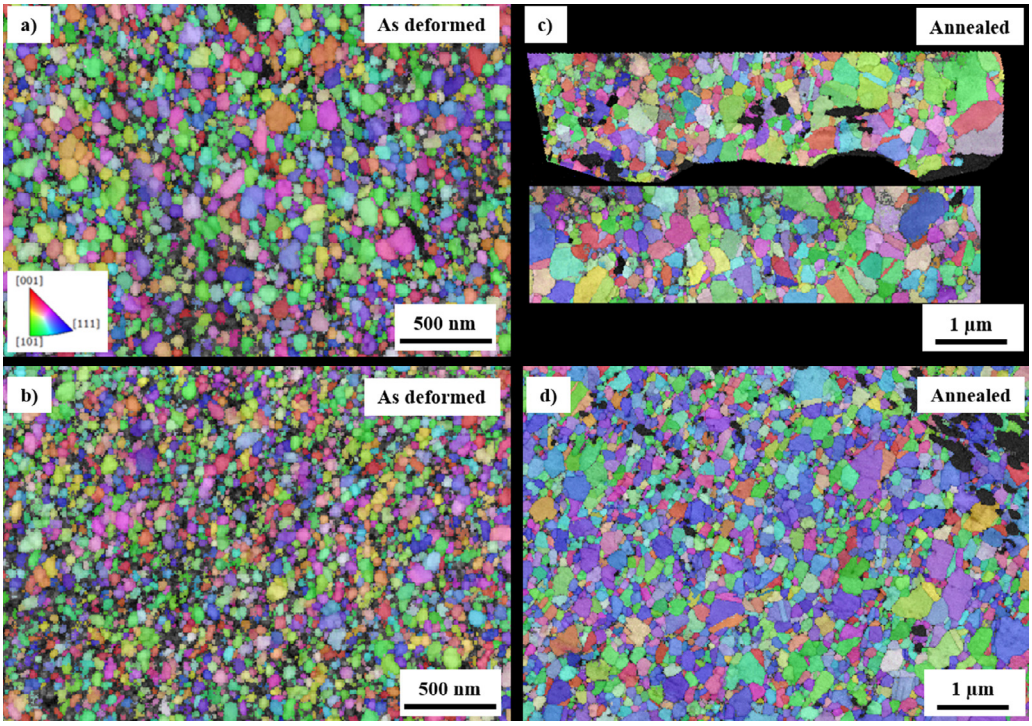


**Fig. 2.** TKD orientation maps (with pattern quality overlay) of Ni-MMCs with 2wt% CNTs in as-deformed state (a,b) and after annealing at 500°C for 3h (c,d): HPT deformed at 200°C (a,c) and HPT deformed at two temperatures (b,d).

with some agglomerates having a diameter of about 1 µm. Larger CNT agglomerates are stretched in the shear direction. The distribution is inhomogeneous with clusters of larger agglomerates inter dispersed by smaller ones. Furthermore, areas with no discernible CNT agglomerates can be identified, especially for Ni-MMCs with low CNT content. The Ni-MMC samples, which were HPT deformed at two temperatures (lower row), show evenly distributed CNT agglomerates with an overall smaller size. There are only a few individual agglomerates at higher CNT concentrations visible, which have a size larger than 1 µm.

To characterize the microstructure as well as the grain size distribution of the Ni matrix after HPT processing, Transmission Kikuchi Diffraction (TKD) in a SEM equipped with a Bruker QUANTAX EBSD system for TKD was performed. Fig. 2 shows representative orientation maps of different deformed states of Ni-MMCs with 2wt% CNTs in axial direction. The Ni matrix consists of nanocrystalline, equiaxed grains, with a similar microstructure for both processing conditions in the as-deformed state. The area weighted grain sizes were determined from the TKD scans. The two-temperature deformation process with 200°C being the second processing temperature resulted in similar grain sizes (96 nm) as the deformation at 200°C alone (85 nm), indicating that the final HPT-deformation temperature determines the final grain size of the Ni matrix. The grain sizes in the MMCs are smaller than in commercial, pure Ni, which is HPT deformed at the same deformation temperature (200°C) [15].

Vickers microhardness measurements of the as-deformed Ni-MMCs were performed using a load of 300g (HV0.3). The sat-

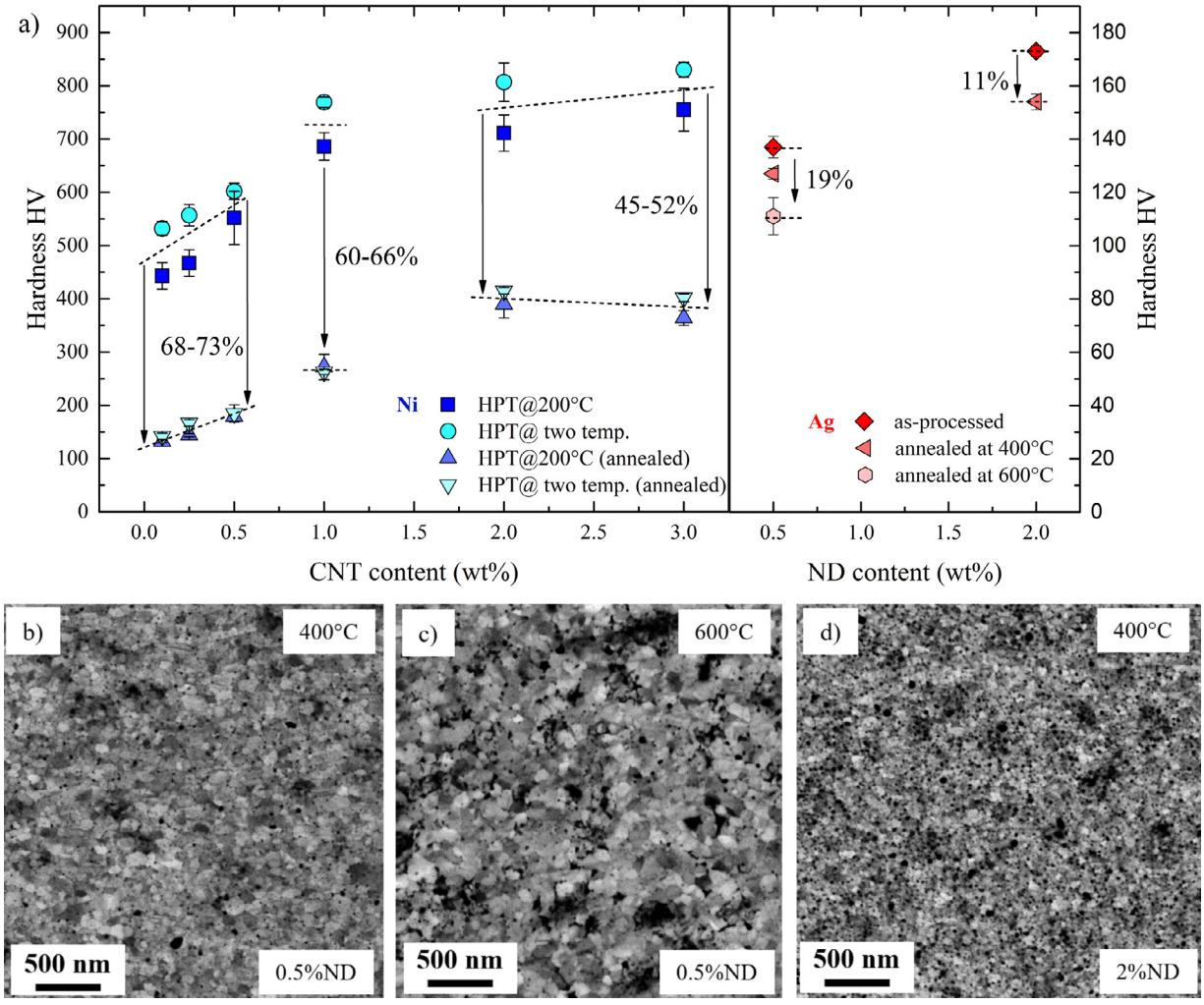


**Fig. 3.** a) Vickers microhardness as a function of the CNT and ND content for as-deformed and annealed Ni- and Ag-MMCs. The Ni-MMCs are HPT-deformed at 200°C and with two temperatures. SEM images of Ag-MMCs with 0.5wt%NDs after annealing at b) 400°C (0.54 $T_m$) and c) 600°C (0.71$T_m$) for 2h and d) 2wt% NDs after annealing at 400°C for 2h.

uration microhardness ranges between 575 and 830HV in the as-deformed state (Fig. 3a). The significantly finer microstructure compared to pure Ni is also evidenced by the higher hardness of the as-deformed Ni-MMCs, as pure Ni HPT deformed at 200°C reaches a smaller saturation microhardness of about 450HV [15]. Although similar grain sizes are achieved in the Ni-MMCs independent of the HPT processing conditions, the microhardness is about 75HV lower in the sample deformed at 200°C than in the samples deformed with the two-temperature process (Fig. 3a). This hardness difference might be attributed to the improved distribution and smaller size of the remaining CNT agglomerates. Higher microhardness values in sintered Ni/CNT-MMCs due to a better homogeneity of the reinforcement phase were also found in [16]. For all Ni-MMCs, the microhardness increases with increasing CNT content. This trend does not clearly continue and levels off for higher CNT concentrations, which seems to be caused by the increase of the size of the agglomerates.

After HPT deformation, the deformed Ni-MMCs were additionally heat treated for 3h at 500°C (0.45$T_m$) in vacuum to investigate their thermal stability. In Fig. 3a, the microhardness evolution after annealing as a function of the CNT content is presented as well. It can be seen that the microhardness significantly decreases after annealing for all Ni-MMCs. Independent of the used HPT processing, similar microhardness values are reached after annealing for each CNT concentration.

TKD analysis was used to characterize the microstructure of annealed Ni-MMCs with 2wt% CNTs (Fig. 2c,d). In agreement with the microhardness measurements, grain coarsening is observed, but no obvious structural difference between the annealed states depending on HPT processing and improved CNT distribution can be determined. Average equivalent grain sizes of 276nm (deformation temperature 200°C) and 333nm (two-temperature deformation) are maintained after annealing. In [17], the thermal stability of pure HPT deformed Ni powder was evaluated. Despite a lower annealing temperature (3h at 300°C (0.33$T_m$)), the pure Ni sample showed significant microstructural coarsening and abnormal grain growth after the heat treatment. To illustrate the influence of the CNT content, the relative microhardness reduction can be calculated. For Ni-MMCs with low CNT contents (0.1-0.5wt%), the microhardness after annealing decreases by about 70%. The microhardness reduction is still quite high (~65%) for Ni-MMCs containing 1wt% CNTs. For higher CNT contents (2 and 3wt%), however, the microhardness only drops to about one half. From the microstructural investigations and microhardness results it seems that the improved CNT distribution on the macroscale after deformation at two temperatures has no significant influence on the thermal stability, whereas the amount of added CNTs slightly affects stability.

In general, however, the microstructure remains significantly finer compared to pure Ni [17,18].

To investigate the influence of a different type of nanocarbon reinforcement on thermal stability, Ag-MMCs with 0.5 and 2wt% NDs were processed by HPT deformation using Ag powder (Alfa Aesar, 500 mesh, spherical) and ND powder (Plasmachem, particle size: 4-6 nm) as described in [14]. Ball milling of Ag-ND powder blends was used to break up ND agglomerates before HPT deformation at room temperature (similar homologous temperature to the final deformation temperature of Ni-MMCs) [14]. In the Ag-MMCs, a homogeneous dispersion of the NDs in the Ag matrix is achieved on the macroscale. With increasing ND content, significantly finer Ag grain sizes can be achieved (68 nm with 0.5wt%NDs, 43 nm with 2wt%NDs), which lead to a high microhardness of 137HV (0.5wt%NDs) and 173HV (2wt%NDs). After processing, the Ag-MMCs were heat treated at similar homologous temperatures (at 400°C for 2h ($0.54T_m$)) as the Ni-MMCs. After annealing, nearly no change in microstructure is observed for both compositions, which is further reflected in an almost constant microhardness (Fig. 3). In contrast to the Ni-MMCs reinforced with CNTs, the microhardness decreases by 7 and 11%, respectively. Therefore, the Ag-MMC with 0.5wt% ND was also annealed at higher homologous temperatures (600°C ($0.71T_m$)) for 2h and slight grain coarsening of the Ag matrix is observed (Fig. 3c). Despite the structural coarsening, the measured hardness of 111HV is still 81% of the hardness of the as-deformed Ag-MMC. To assess the effectiveness of the NDs to stabilize the microstructure, pure Ag powder samples were HPT processed and annealed with the same parameters. In the as-deformed state, a NC microstructure with a microhardness of 104HV is obtained [14]. After annealing, similar hardness values, 57HV (annealed at 400°C) and 51HV (annealed at 600°C), are measured for both samples. The microhardness after annealing is distinctly lower compared to the Ag-MMCs, which indicates a lower thermal stability of the pure Ag samples.

To understand the difference in thermal stability depending on the type of nanocarbon reinforcements, transmission electron microscopy (TEM) investigations in a JEOL 2100F instrument were performed to determine the nanocarbon distribution at the nanoscale. Fig. 4 shows TEM images of both investigated Ni-MMCs with 2wt% CNTs and the Ag-MMC reinforced with 2wt% NDs. To determine the size of CNT and ND agglomerates and estimate their volume fraction, particle analysis on several TEM images with the program ImageJ was performed [19,20]. After HPT deformation at 200°C, nanometer sized as well as larger CNT agglomerates, which are rather poorly distributed, can be seen in the Ni matrix (the CNTs identified unambiguously are indicated in Fig. 4a). The mean size of the CNT agglomerates is 41.3±43 nm. Many of the CNT agglomerates are irregularly shaped. From high-resolution TEM images, it is visible that they consist of many multi-walled CNT fragments, sticking together with no preferred orientation (Fig. 4b). The interface between the Ni matrix and CNT agglomerates shows a good bonding. Overall, the CNT agglomerates are smaller (37.3±20 nm) and more homogeneously distributed in the Ni matrix in the sample deformed by the two-temperature process (Fig. 4c). However, the distance to each other is rather large. The internal structure shows a fingerprint-like appearance of CNT fragments (Fig. 4d). Again, there is no visible porosity at the interface between the two phases. The spacing's between the individual CNT layers have been measured to be 0.37 ± 0.03 nm (200°C) and 0.41 ± 0.05 nm (400°C+200°C). These values are slightly larger than the 0.34 nm measured in pristine multi-walled CNTs [21]. For both Ni-MMCs, the CNT agglomerates are in the same size range or even larger as the Ni matrix grains. Their volume fraction is 4.8% for the Ni-MMC HPT-deformed at 200°C and 2.5% for the Ni-MMC HPT deformed by the two-temperature process. The Fig. 4e shows the Ag-MMC with 2% NDs in the as-deformed state. The magnification is twice as large compared to the Ni-MMCs. In the Ag-MMC, the ND agglomerates are homogeneously distributed at the nanoscale and located at grain boundaries and triple junctions of the Ag matrix grains (Fig. 4e). In case of the Ag-MMCs, the size of the ND agglomerates is much smaller (15.7±8 nm) than the grain size of the Ag matrix. The ND agglomerate volume fraction is 3.7%. In Fig. 4f, a high-resolution TEM image of such a ND agglomerate located at a triple junction is shown. It consists of several NDs separated by an amorphous carbon grain boundary phase.

The thermal stability of nanocrystalline materials can be enhanced using different strategies [22–28]. Kinetic stabilization arises from reduced grain boundary mobility, whereby grain boundaries can be pinned in various ways, e.g. second phase Zener drag [29] or solute (impurity) drag [30–32]. A previous study of our group revealed that irreversible damage to CNTs in HPT deformed MMCs is already introduced at low levels of strain [33]. During HPT deformation, the CNTs undergo an amorphization trajectory following a model as proposed in [34]. It can therefore be expected that sufficient carbon atoms are available after deformation as impurities in the Ni-MMCs, as a consequence of this irreversible damage [33]. It can also be assumed that single carbon atoms are removed from NDs and dissolved in the Ag matrix during ball milling and subsequent HPT deformation [14], although it is more unlikely due to the predominance $\sigma$-bonds, which are very stable [35]. In [15] it was shown that the saturation grain size of HPT-deformed Ni further depends on the carbon content, with an increasing amount of carbon leading to an increase in hardness and finer microstructures consistent with the results on Ni-MMCs. Atom probe investigations indicated that carbon is dispersed along the grain boundaries in HPT deformed Ni [15]. Due to the small size and low solubility of carbon in Ni and Ag [36–38], segregation to interfaces like grain boundaries can be expected in the HPT deformed MMCs stabilizing the nanostructure of the matrix by the solute drag mechanism. Carbon segregation to grain boundaries might also contribute to a stabilization of grain size by reducing the grain boundary energy (thermodynamic stabilization mechanism [26,39]). X-ray diffraction in-situ annealing experiments revealed carbide formation ($Ni_3C$) between 200°C and 350°C in CNT reinforced HPT deformed Ni-MMCs, which are metastable and decompose above 350°C [10]. The observed carbide formation can affect the thermal stability in two possible ways: $Ni_3C$ can reduce the grain boundary mobility by exerting a pinning force, but can also leads to a possibly reduced thermodynamic and solute drag stabilization mechanism by the loss of carbon at grain boundaries. Indeed, it could be shown that the grain growth rate of the Ni matrix is nearly zero up to 350°C and increases after decomposition of $Ni_3C$ during in-situ annealing [10].

Our results demonstrate a superior thermal stability of MMCs reinforced with NDs compared to the use of CNTs as reinforcement phase. The matrix grain size of the HPT processed Ag-MMCs remains very stable with sizes of about 100 nm after annealing at 600°C ($0.71T_m$) for 2 h. This fits well to reported maximum homologous temperatures that can be attained without coarsening in nanocrystalline materials reinforced by different nanosized particles [23]. Adding CNTs, however, does not efficiently stabilize the nanocrystalline Ni matrix grains and significant coarsening is already observed after annealing at lower homologous temperatures ($0.45T_m$) in the Ni-MMCs.

To achieve a maximum pinning force by second phase particles, a small particle size and a high volume fraction are required according to classical Zener pinning [23,29]. Additionally, the spatial distribution of the particles should be as uniform as possible. A further crucial factor is a sufficient resistance against coarsening at elevated temperatures.

In the Ni-MMCs, CNT agglomerates exist at the macro- and nanoscale for all CNT concentrations. The hardness reduction,

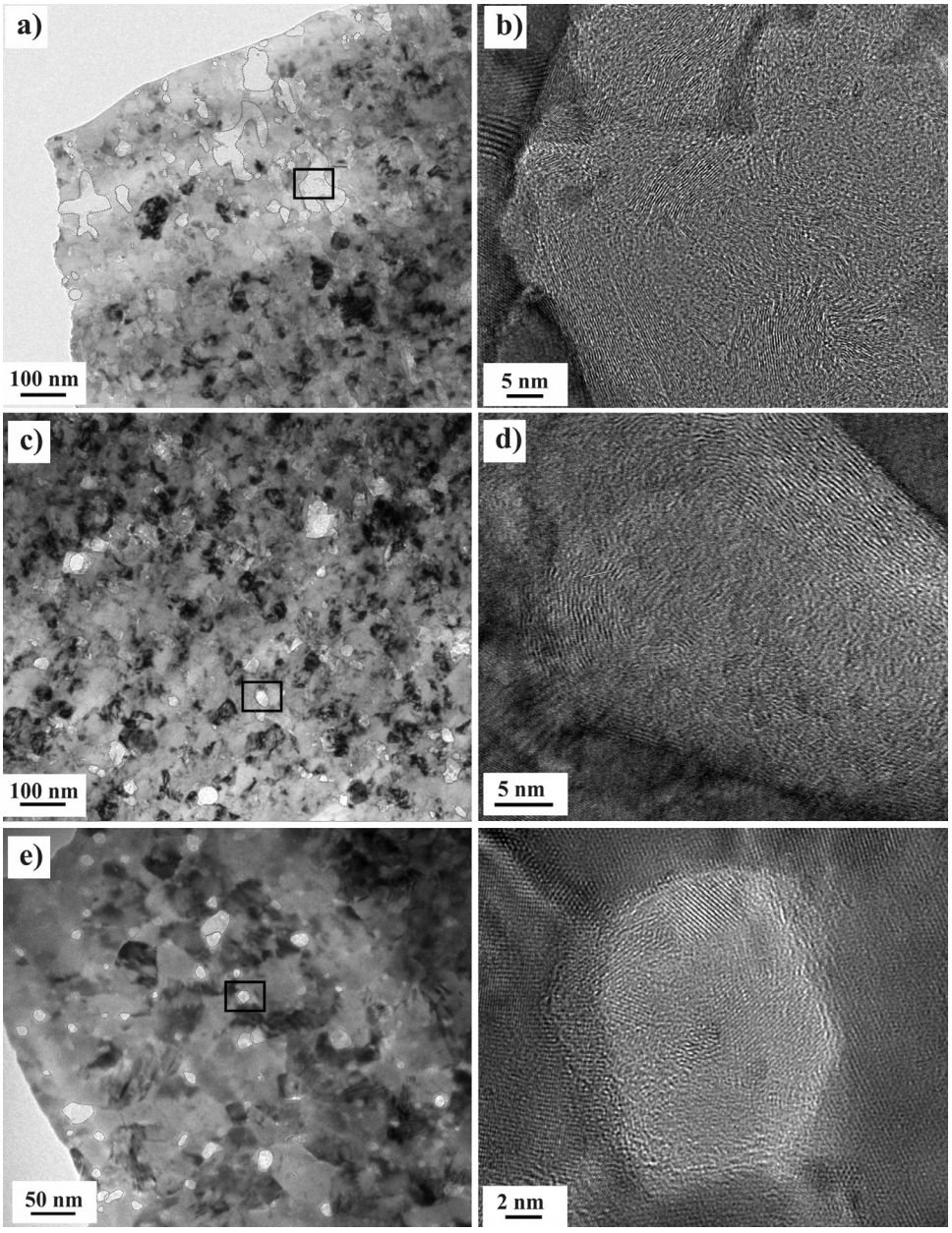


**Fig. 4.** TEM and high-resolution TEM images of Ni with 2wt% CNTs HPT-deformed at 200°C (a, b) and with two temperatures (c, d) and of Ag with 2wt% NDs HPT deformed at RT (e,f). CNT and ND agglomerates, which could be unambiguously identified, are marked. The black boxes mark regions, where the high-resolution images were taken.

which can be correlated to structural coarsening, is slightly less for higher CNT contents (Fig. 3a). However, no significant difference between CNT concentrations of 2 and 3% is found. In particular, at higher CNT concentrations, most of the CNTs are accumulated in agglomerates, which are much larger than the Ni grain size. As a consequence, the amount of nanosized CNT clusters present at individual grain boundaries and triple junctions does not necessarily increase with the overall CNT content. Although a better distribution is achieved at the macroscale after the two temperature process (Fig. 1), an inhomogeneous distribution is still persistent at the nanoscale (Fig. 4c). Thus, the CNT agglomerates do not provide effective stabilization of the nanostructures by the particle pinning mechanism.

By contrast, the smaller agglomerate size and the uniform distribution of the NDs increase the effectiveness of the stabilization by particle pinning in Ag-MMCs (Fig. 3b and Fig. 4). Since the CNT agglomerates volume fraction is similar to the volume fraction of the ND agglomerates in the microstructure, the essential factors leading to a better thermal stability are the uniform spatial distribution and the smaller size of the NDs.

In summary, the high grain size stability of Ag-MMCs is considered to be due to the pinning forces arising from impurities (carbon) as well as homogeneously dispersed NDs. Additionally, only a low volume fraction (0.5wt% ND corresponds to only 1.6vol.% NDs) is needed for thermal stabilization even at high homologous temperature ($>0.7T_m$). The 0.5wt% ND reinforced Ag-MMC further presented a remarkable strength over pure Ag with tensile strength values exceeding 400 MPa and a good ductility [14], which is also essential for possible future applications.

A. Bachmaier and A. Katzensteiner gratefully acknowledge the financial support by the Austrian Science Fund (FWF): I2294-N36. K. Aristizabal wishes to thank the German Academic Exchange Service (DAAD) (91567148) for their financial support. S. Suarez and K. Aristizabal gratefully acknowledge the financial support from DFG

(Grant: SU911/1-1). This project received funding from the European Research Council (ERC) under the European Union's Horizon 2020 research and innovation programme (Grant No. 757333). The authors thank K. Kormout for TEM investigations.

## Declaration of Competing Interest

The authors declare that they have no known competing financial interests or personal relationships that could have appeared to influence the work reported in this paper.

## References

[1] A. Mortensen, J. Llorca, Annu. Rev. Mater. Res. 40 (2010) 243–270.
[2] R. Anish, G.R. Singh, M. Sivapragash, Proc. Eng 38 (2012) 3846–3854.
[3] R. Valiev, R. Islamgaliev, I. Alexandrov, Prog. Mater. Sci. 45 (2000) 103–189.
[4] A. Bachmaier, R. Pippan, Int. Mater. Rev. 58 (2013) 41–62.
[5] S.R. Bakshi, D. Lahiri, A. Agarwal, Int. Mater. Rev. 55 (2010) 41–64.
[6] P. Jenei, J. Gubicza, E.Y. Yoon, H.S. Kim, J.L. Lábár, Compos. Part A Appl. Sci. Manuf. 51 (2013) 71–79.
[7] S. Suarez, F. Lasserre, F. Soldera, R. Pippan, F. Mücklich, Mater. Sci. Eng. A 626 (2015) 122–127.
[8] S. Suárez, E. Ramos-Moore, B. Lechthaler, F. Mücklich, Carbon N. Y. 70 (2014) 173–178.
[9] D.D. Phuong, P. Van Trinh, N. Van An, N. Van Luan, P.N. Minh, R.K. Khisamov, K.S. Nazarov, L.R. Zubairov, R.R. Mulyukov, A.A. Nazarov, J. Alloys Compd. 613 (2014) 68–73.
[10] K. Aristizabal, A. Katzensteiner, A. Bachmaier, F. Mücklich, S. Suárez, Sci. Rep. 10 (2020) 857.
[11] V.A. Popov, E.V Shelekhov, E.V Vershinina, Eur. J. Inorg. Chem 2016 (2016) 2122–2124.
[12] A. Katzensteiner, T. Müller, K. Kormout, K. Aristizabal, S. Suarez, R. Pippan, A. Bachmaier, Adv. Eng. Mater. 21 (2019) 1800422.
[13] K. Aristizabal, A. Katzensteiner, A. Bachmaier, F. Mücklich, S. Suárez, Mater. Charact. 136 (2018) 375–381.
[14] A. Katzensteiner, J.M. Rosalie, R. Pippan, A. Bachmaier, Mater. Sci. Eng. A (2020) 139254.
[15] G.B. Rathmayr, R. Pippan, Acta Mater 59 (2011) 7228–7240.
[16] P. Rossi, S. Suarez, F. Soldera, F. Mücklich, Adv. Eng. Mater. 17 (2015) 1017–1021.
[17] S. Suarez, F. Lasserre, F. Soldera, R. Pippan, F. Mücklich, Mater. Sci. Eng. A 626 (2015) 122–127.
[18] E. Schafler, R. Pippan, Mater. Sci. Eng. A 387–389 (2004) 799–804.
[19] C.A. Schneider, W.S. Rasband, K.W. Eliceiri, Nat. Methods 9 (2012) 671.
[20] J.J. Friel, in: Practical Guide to Image Analysis, ASM International, 2000, pp. 19–22.
[21] S. Iijima, Nature 354 (1991) 56–58.
[22] H.R. Peng, M.M. Gong, Y.Z. Chen, F. Liu, Int. Mater. Rev. 62 (2017) 303–333.
[23] C.C. Koch, R.O. Scattergood, M. Saber, H. Kotan, J. Mater. Res. 28 (2013) 1785–1791.
[24] C.C. Koch, R.O. Scattergood, K.A. Darling, J.E. Semones, J. Mater. Sci. 43 (2008) 7264–7272.
[25] T. Chookajorn, H.A. Murdoch, C.A. Schuh, Science 337 (2012) 951–954.
[26] H.A. Murdoch, C.A. Schuh, J. Mater. Res. 28 (2013) 2154–2163.
[27] T.R. Malow, C.C. Koch, Mater. Sci. Forum 225–227 (1996) 595–604.
[28] R.A. Andrievski, J. Mater. Sci. 49 (2014) 1449–1460.
[29] P.A. Manohar, M. Ferry, T. Chandra, ISIJ Int 38 (1998) 913–924.
[30] G. Gottstein, D.A. Molodov, L.S. Shvindlerman, Interface Sci 6 (1998) 7–22.
[31] K. Lücke, H. Stüwe, Acta Metall 19 (1971) 1087–1099.
[32] J.W. Cahn, Acta Metall 10 (1962) 789–798.
[33] K. Aristizabal, A. Katzensteiner, A. Bachmaier, F. Mücklich, S. Suarez, Carbon 125 (2017) 156–161.
[34] A.C. Ferrari, J. Robertson, Phys. Rev. B 61 (2000) 14095–14107.
[35] H.O. Pierson, in: Handbook of Carbon, Graphite, Diamonds and Fullerenes. Processing, Properties and Applications, Noyes Publications, 1993, pp. 11–42.
[36] H. Ohtani, M. Hasebe, T. Nishizawa, Trans. ISIJ 24 (1984) 857–864.
[37] R.B. McLellan, Scr. Metall. 3 (1969) 389–391.
[38] I. Karakaya, W.T. Thompson, Bull. Alloy Phase Diagrams 9 (1988) 226–227.
[39] M. Saber, C.C. Koch, R.O. Scattergood, Mater. Res. Lett. 3 (2015) 65–75.